IABSE TG3. 1 final analysis: Comparison between full-scale measurements and numerical simulations of a long-span bridge

IABSE TG3.1 final analysis: Comparison between full-scale measurements and numerical simulations of a long-span bridge during a non-synoptic event

Giorgio Diana

Politecnico di Milano, Milan, IT

Stoyan Stoyanoff

RWDI, Guelph, Canada

And other TG3.1 Members: Tommaso Argentini, Niccolò Barni, Filippo Calamelli, Miguel Cid Montoya, Santiago Hernández, Allan Larsen, Claudio Mannini, Daniele Rocchi, Roberto Rossi, Martin Svendsen, Teng Wu

Contacts: giorgio.diana@polimi.it, stoyan.stoyanoff@rwdi.com, tommaso.argentini@polimi.it, niccolo.barni@unifi.it, filippo.calamelli@polimi.it,mcidmon@clemson.edu,santiago.hernandez@udc.es,aln@cowi.dk, claudio.mannini@unifi.it, daniele.rocchi@polimi.it, roberto1.rossi@polimi.it, mnns@ramboll.dk, tengwu@buffalo.edu

Abstract

Over the past few years, the frequency and intensity of extreme climate events such as thunderstorms and downbursts have increased. These non-synoptic events involve large fluctuations in wind speed and angle of attack, potentially inducing critical conditions for bridge decks. Technological advancements in full-scale monitoring have not only confirmed these characteristics but have also enabled deeper investigations of long-span bridges aeroelastic behavior. These circumstances have proven to be a valuable opportunity for the IABSE TG3.1, which has been involved for the past 6 years in benchmarking software to compute bridge responses to turbulent winds, to extend the validation of numerical methods to extreme weather phenomena. To achieve this goal, it was decided to compare the results of numerical simulations obtained by the participants with the measured full-scale response of the Hardanger Bridge during the storm “Tor”, which struck the bridge in 2016. To provide a suitable input for the simulations, wind tunnel tests were carried out in the Politecnico di Milano wind tunnel on a deck sectional model of the bridge. This paper presents the first numerical results and compares them with the monitored bridge response.

Keywords: Long-span bridges, aeroelasticity, non-synoptic winds, numerical methods

1 Introduction

In recent decades, the impact of climate change has become increasingly evident, leading to a rise in the frequency and intensity of extreme climate phenomena, such as thunderstorms and downbursts. The inherently localized and dynamic nature of these events presents significant challenges in understanding their impact on the aeroelastic response of bridges. Specifically, unlike standard synoptic winds, non-synoptic phenomena are frequently characterized by rapid and marked fluctuations in wind speed and angle of attack [1][11]. Depending on the deck aerodynamic characteristics, these features can lead to nonlinearities in the wind forces, which can significantly impact the response of long-span bridges [4].

Technological progress in full-scale monitoring has both confirmed these findings and opened the door to more comprehensive studies on the aeroelastic behavior of long-span bridges. These circumstances have proven to be a valuable opportunity for IABSE Task Group 3.1, which has been involved for the past years in benchmarking software to compute bridge responses to turbulent

winds [7][8][9], to extend the validation of numerical methods to extreme weather phenomena. The monitoring campaign carried out on the Hardanger Bridge in Norway provided an outstanding case study to reach this purpose [11]. The bridge was equipped with several anemometers and accelerometers distributed along the deck, enabling the recording of both the incoming wind and the corresponding structural response. In particular, recordings of the storm "Tor", which hit the coast of Norway in January 2016, were selected as characterized by pronounced variation of the wind speed and angle of attack. The main target of this IABSE TG3.1 final step is to compare numerical results, obtained by the participants, with the full-scale measured response of the bridge during the storm.

Defining the inputs for simulating this case study is challenging, and several issues must be addressed. One of the primary difficulties lies in generating a numerical wind scenario that accurately represents full-scale conditions. Specifically, to perform the calculations, a wind time-space distribution is required. However, the storm was recorded only at a few specific sections, corresponding to the locations of the anemometers along the deck. As a result, determining the turbulence characteristics necessary for generating the synthetic wind scenario is particularly challenging in this non-synoptic case study, which features highly localized wind properties. Furthermore, as reported by [10], anemometer measurements may be affected by the presence of the deck itself.

To evaluate this effect and determine the deck aerodynamic properties, i.e. static coefficients and flutter derivatives, experimental tests were conducted in the Politecnico di Milano wind tunnel on a deck sectional model. Moreover, to verify that the structure's response during storm "Tor" was not influenced by vortex shedding, the sectional model was suspended on springs to assess the deck's susceptibility to this Vortex-Induced Vibrations (VIV).

After completing the wind tunnel tests and generating a synthetic non-synoptic wind scenario representative of the storm, the input data were shared with all benchmark participants to perform the simulations. As previously mentioned, the significant variations in wind speed and angle of attack induce nonlinearities in the aerodynamic forces, which may significantly impact the bridge's aeroelastic response. Therefore, it is essential to employ computational algorithms capable to capture these nonlinear effects. [2] [4].

This paper briefly describes the Hardanger Bridge monitoring campaign along with the characteristics of the storm selected as a case study. Subsequently, the wind tunnel tests performed are detailed and finally, the first numerical results are shown and compared with the full-scale response of the bridge.

2 Hardanger Bridge monitoring campaign and storm "Tor"

The Hardanger Bridge, located in Norway, features a single-span of 1308 m. The deck consists of a single-box section with a chord 18.3 m wide (see Figure 1). A monitoring system, including 16 accelerometers and 8 anemometers positioned along the deck, was installed on the bridge shortly after its public opening in 2013. The accelerometers were placed on both sides of the deck to capture its torsional rotation. Except for the midspan one, the anemometers were primarily installed on the hangers along the bike lane side, 8 meters above road level, to facilitate maintenance. In contrast, the midspan anemometer was positioned on the road lane side. (refer to [11] for the specific locations of the sensors)

The Norwegian coastline, and specifically the Hardanger Bridge, was hit by an extratropical cyclone, named "Storm Tor", between January 29 and 30. The wind characteristics and the corresponding structural response were recorded by the monitoring system installed on the bridge. Figure 2 shows the wind longitudinal component u and the angle of attack (defined as $AoA = \tan^{-1}\left(\frac{w}{u}\right)$, where w is the vertical wind component) acquired by the midspan anemometer between 16:30 and 17:00 on January 29th. It can be observed that both u and AoA exhibit significant low-frequency variations: the wind speed increases from approximately 15 m/s to more than 35 m/s within 200 s, while the angle of attack exceeds 10°.

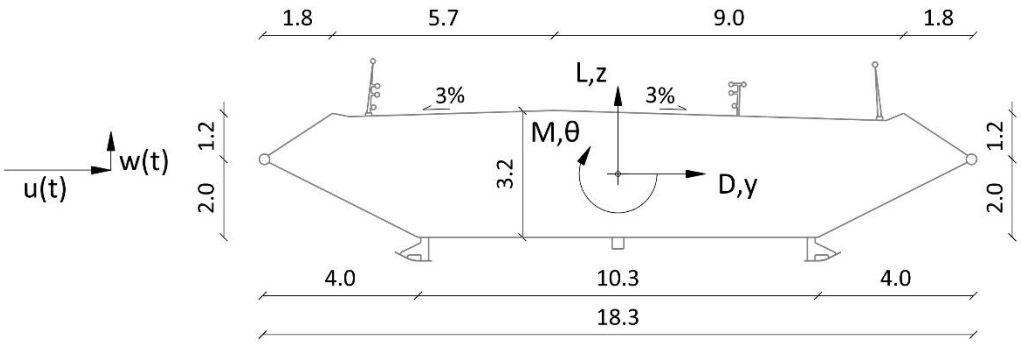

Figure 1. Deck section of the Hardanger Bridge and sign convention

As mentioned in the Introduction, these large low-frequency wind oscillations can induce nonlinearities in the aerodynamic forces which can lead to significant changes in the bridge response.

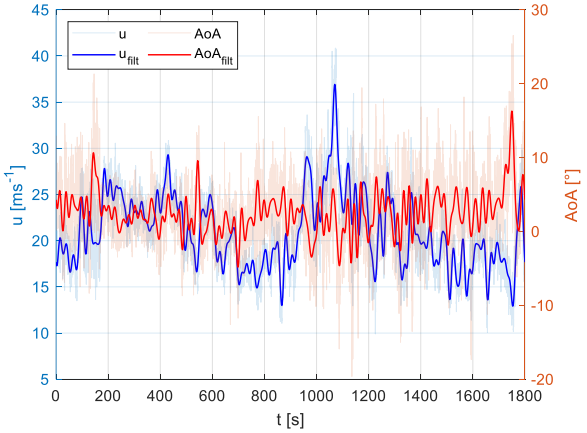

Figure 2. Wind speed and angle of attack recorded by the midspan anemometer during the storm "Tor". The signals labeled as "filt" have been low-pass filtered with a cutoff frequency of 0.06 Hz

This time sequence was selected by the research group as a benchmark non-synoptic case study to be simulated, aiming to extend the validation of numerical methods to predict the aeroelastic response of bridges to extreme weather events. To define aerodynamic input data suitable for simulating this scenario, dedicated tests were carried out in the Politecnico di Milano wind tunnel.

3 Wind tunnel tests

3.1 Static aerodynamic coefficients and flutter derivatives

To numerically simulate the aeroelastic response of the Hardanger Bridge, the deck aerodynamic characteristics are required. Specifically, static aerodynamic coefficients and flutter derivatives were measured positioning a deck sectional model (scale 1:18) on dynamometric balances (see Figure 3). To simulate the effects induced by the high angles of attack reached during the storm (see Figure 2), drag, lift and moment coefficients (i.e. C_D, C_L and C_M, defined as reported by [6]) were evaluated over an AoA range from -15° to 15° and wind speeds from 8 m/s to 20 m/s. Moreover, since the storm was coming from the North Sea, the coefficients were measured from the road lane side, which is oriented in this direction. The values obtained are shown in Figure 4. First, it can be observed that no significant changes are induced by the wind speed variation (i.e. Reynolds number $Re = \frac{UB}{\nu}$, with $\nu = 1.5 \times 10^{-5}\, m^2/s$ air kinematic viscosity, ranging from 5.4×10^5 to 1.4×10^6). Furthermore, the derivatives of C_L and C_M with respect to the AoA decrease approaching 5°.

Flutter derivatives were evaluated using the forced motion method, following the procedure outlined by [6].

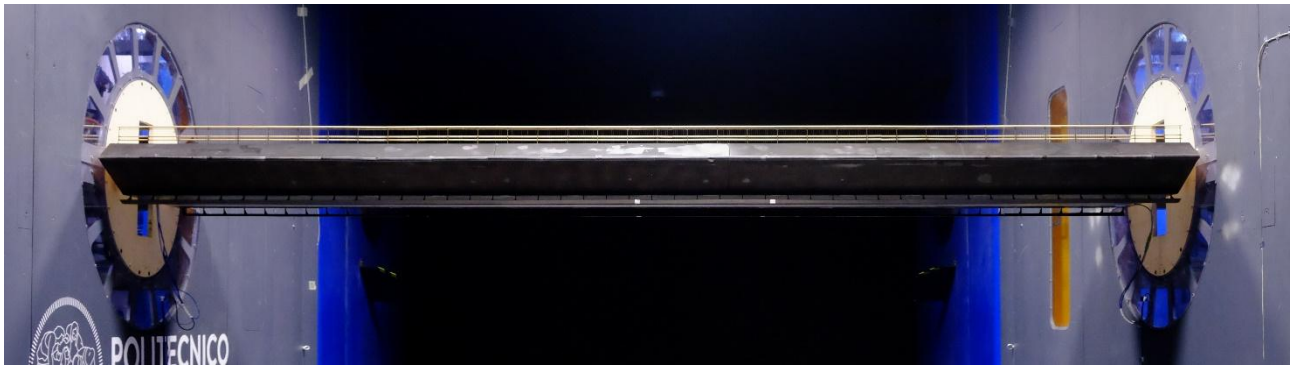

Figure 3. Deck sectional model of the Hardanger Bridge on dynamometric balances

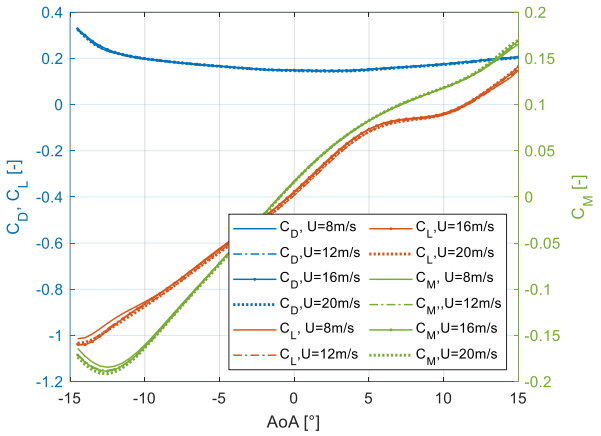

Figure 4. Drag, lift and moment coefficients, as a function of the AoA, measured for different mean wind speeds

The range of reduced velocities (i.e. $V^* = \frac{U}{fB}$, where f is the deck oscillation frequency), investigated is distinguished based on the forced motion imposed. The values were calculated by separately considering the oscillation frequencies of the deck's main lateral, vertical, and torsional vibration modes, and the wind speed values observed during the storm (refer to Figure 2). Specifically, coefficients obtained from lateral harmonic motion are identified within V^* values between 6 and 40, those from vertical harmonic motion between 2.4 and 40 and those from torsional motion between 1.5 and 40. As for the static aerodynamic coefficients, since high wind angles occur during the non-synoptic event under analysis, flutter derivatives were identified within a range of static deck rotations between -9° and 9°. Figure 5 and Figure 6 show, as an example, the coefficients a_2^* and a_3^*, defined according to the formulation reported by [12], as a function of V^* for different deck static angles of rotation. It can be observed that a_2^* becomes negative for $AoA \geq 3°$. According to [12], a negative value of this coefficient represents negative aerodynamic damping, which can lead to a one-degree-of-freedom torsional instability. It is worth mentioning that the values related to deck static rotations equal to 1.5° and 4.5° are identified within a limited V^* range, as they were measured a posteriori to refine the coefficients' trend as a function of the AoA.

To avoid numerical issues in the simulation, flutter derivatives were fitted using rational functions. The outcome of the fitting procedure is also reported in Figure 5 and Figure 6.

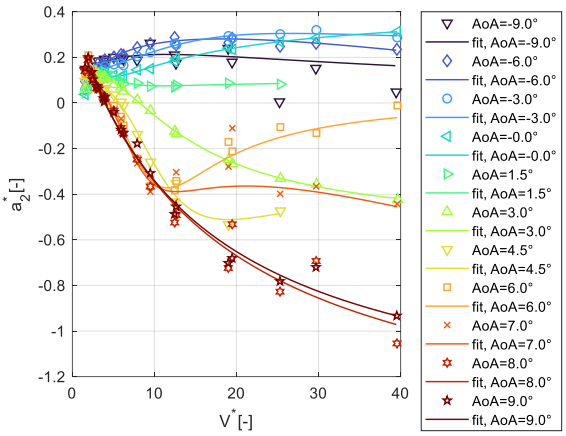

Figure 5. a_2^* coefficients as a function of V^* for different deck static angles of rotation

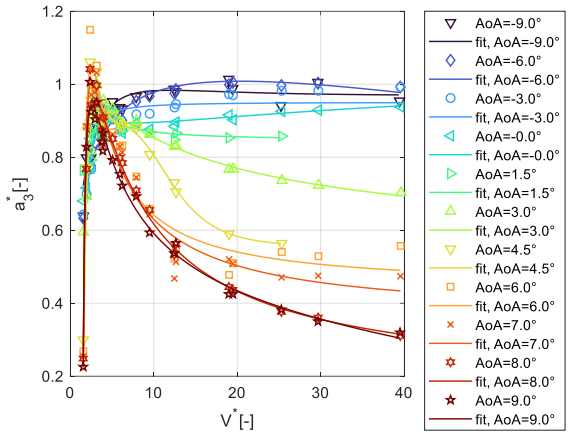

Figure 6. a_3^* coefficients as a function of V^* for different deck static angles of rotation

3.2 Correction of the anemometers' measurements

As reported by [10], the wind signals recorded by the anemometers installed on bridge decks can be influenced by the presence of the structure itself. To evaluate this effect for the instrumentation installed on the Hardanger Bridge, Computational Fluid Dynamics (CFD) simulations were preliminarily conducted. Specifically, two-dimensional steady RANS simulations of the deck were carried out to analyze the deviation of the incoming wind at the locations of the anemometers, which are connected to the hangers, 8 m above the road level (refer to [11]). The correction to be applied to the full-scale measured wind angle is evaluated as

$$corr = AoA_{wind} - AoA_{measured} \quad (1)$$

where AoA_{wind} is the angle of attack of the approaching wind while, $AoA_{measured}$ is that numerically recorded at the anemometer's location. Therefore, if $AoA_{measured}$ is the wind angle measured by the full-scale anemometer, the following equation needs to be applied to account for the flow deflection induced by the presence of the deck itself

$$AoA_{wind} = AoA_{measured} + corr \quad (2)$$

This result was experimentally validated through wind tunnel tests. Specifically, a cobra probe was positioned at the full-scale location of the anemometers to measure the AoA for different deck rotations (see Figure 7).

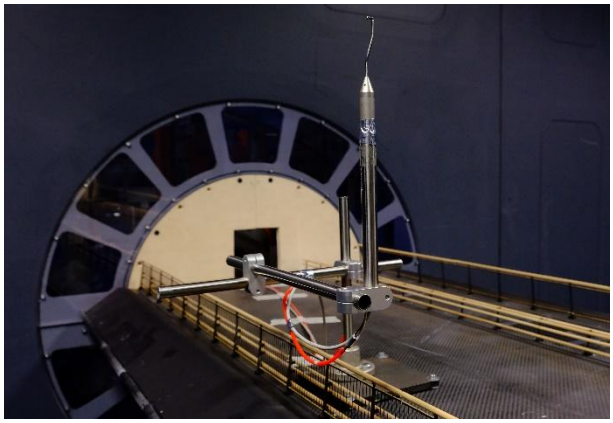

Figure 7. Cobra probe installed on the deck sectional model at the location of the full-scale upwind anemometer

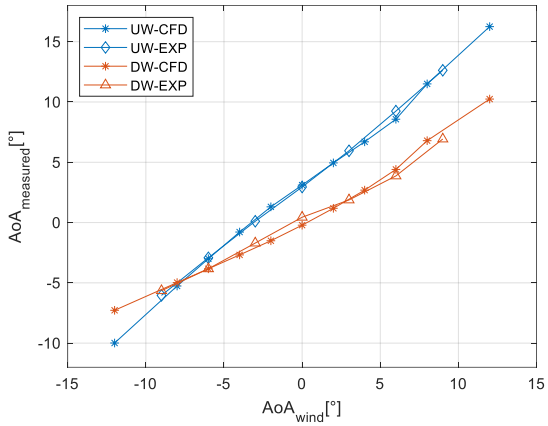

Figure 8. Comparison between numerical and experimental analysis of the wind deflection at the anemometer's location. On the x-axis, the incoming wind AoA is reported while, on the y-axis the AoA, experimentally measured or numerically recorded by performing CFD simulations, is shown

A comparison between experimental and numerical curves is presented in Figure 8. The x-axis shows the incoming wind AoA, while the y-axis reports that measured by the sensor or numerically recorded, both when the anemometer is positioned upwind (UW) and when it is positioned downwind (DW). A good agreement between the curves is observed. The results also show that when the incoming wind is horizontal, i.e. $AoA = 0°$, the flow is deflected upward at the upwind

anemometer but realigns with its initial direction at the downstream location.

Finally, once the wind AoA is corrected according to eq.(2), the vertical velocity component w is adjusted accordingly.

3.3 Vortex-Induced Vibrations

To assess whether there could be any deck oscillation induced by vortex-shedding during the examined non-synoptic event, the deck's susceptibility to VIV is investigated in the wind tunnel, by suspending the sectional model on springs.

VIV is a phenomenon that typically occurs at very low reduced velocities (i.e. $V^* = 0.5 \div 2$). Therefore, the tests focused on the deck's torsional motion, as the wind speed of the examined non-synoptic event, combined with the natural frequencies of the first and second torsional modes ($f_{\theta,1} = 0.37Hz, f_{\theta,2} = 0.55Hz$), results in lower V^* values compared to the vertical one.

A key parameter for VIV is the Scruton number, defined as $Sc = 4\pi\frac{J\zeta}{\rho B^4}$, where J is the deck moment of inertia per unit length, ζ is the damping ratio associated to the motion analyzed and ρ is the air density. To experimentally highlight the phenomenon, Sc is typically kept lower than the target value, by maintaining a lightweight model and low ζ. In these tests, two levels of ζ are considered: the first to achieve a lower Sc than the target, and the second to obtain a comparable value. Moreover, wind AoA between -6° and 6° are investigated.

Table 1. VIV study: main properties of the deck sectional model suspended on springs

Description	Prototype	Model, target	Model, measured
Moment of inertia [kgm²/m]	4.27 x10⁵	4.07	1.90
Frequency [Hz]	-	-	5.52
Damping ratio 1 [-]	0.3	0.3	0.1
Scruton 1 [-]	0.12	0.12	0.02
Damping ratio 2 [-]	0.3	0.3	0.5
Scruton 2 [-]	0.12	0.12	0.09

The properties of the experimental setup are summarized in Table *1*. During the wind tunnel tests, the mean wind speed is gradually increased in small steps, and the steady-state vibrations are measured at each increment.

Figure *9* reports the results obtained, in terms of full-scale vertical oscillations at the edge of deck ($z_{eq} = \theta \tan(B/2)$, where θ represents the deck torsional oscillations).

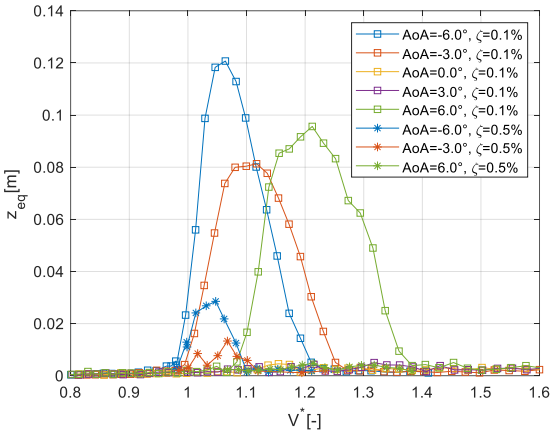

Figure 9. VIV: full-scale equivalent vertical oscillation at the edge of the deck, induced by the torsional motion

The curves show that oscillations due to VIV are recorded mainly for negative angles of attack and when $AoA = 6°$. Moreover, it can be observed that, changing the AoA, the lock-in range occurs at different V^*. Nevertheless, by increasing the damping ratio, the dynamic motion induced by vortex shedding almost disappears. Furthermore, it is important to note that during the storm, V^* values do not drop as low as those at which the phenomenon was observed experimentally.

4 Numerical simulations

This section introduces the inputs used to simulate the Hardanger Bridge's response during the storm "Tor". These inputs were then shared among all IABSE TG3.1 participants to ensure a comparative analysis of the final results given the same initial data.

4.1 Structural properties

The dynamic response of the Hardanger Bridge is numerically simulated by extracting the natural

frequencies, the modal properties and the mode shapes from a Finite Element model of the structure. The study is performed by considering the first 30 modes, whose main features can be found in [3].

4.2 Aerodynamic properties

Static coefficients and flutter derivatives used in this analysis are those presented in Chapter 3.1.

The aerodynamic admittance functions are defined using the Quasi Steady values, introducing the dependency on V^* by the Davenport formulation, defined as

$$A(V^*) = \frac{2}{\left(\frac{7}{V^*}\right)^2}\left(\frac{7}{V^*} - 1 + e^{-7/V^*}\right) \quad (3)$$

It is important to note that $A(V^*)$ is an analytical approximation that not always accurately capture the nonlinearity of the buffeting forces as a function of V^* [6].

4.3 Generation of a non-synoptic wind scenario from full-scale measurements

To simulate the aeroelastic response of a bridge, the time-space distribution of the incoming wind is required. Nevertheless, in the case of a non-synoptic event, which typically exhibits temporal and spatial variations in its characteristics, this task remains challenging and an open area of research.

To achieve this target, the starting point is the anemometer's recordings performed during the storm. As first, the time-series are corrected as reported in Section 3.2. Subsequently, in the deck sections corresponding to the full-scale location of the anemometers, the wind is directly applied to the FE model of the structure. On the other hand, to generate the wind in the intermediate sections (i.e. one section every 20 m along the deck), the following steps were carried out:

- The procedure involves dividing the wind into a low-frequency (LF) and a high-frequency (HF) part, as these exhibit significantly different characteristics. The LF portion is obtained by low-pass filtering the full-scale recorded signals using a cutoff frequency equal to $f_{cut} = \frac{U}{V^*_{cut}B} = \frac{22}{20*18.3} = 0.06Hz$, where $U = 22m/s$ is the mean value of all the anemometer's measurements while the limiting V^*_{cut} value is set equal to 20. It is worth mentioning that the definition of f_{cut} remains subject of discussion in the literature. In this study, the procedure outlined by [5] is adopted. After filtering the signals, the LF wind in the intermediate sections was obtained by linearly interpolating the full-scale measured data;
- As for the HF wind portions, they are generated by considering the turbulence properties during the gust (i.e., referring to Figure 2, by considering the period between 800s and 1400s). The spatial correlation, in this time interval, is assessed by considering the anemometers "A2", "A3", "A4" and "A5", which are close enough to perform an adequate estimate (refer to [11]);
- Finally, the LF and the HF parts are superimposed.

5 Results and discussion

In this Chapter, the results obtained by the participants are presented and compared to the full-scale response of the Hardanger Bridge.

Figure 10(a), Figure 10(b) and Figure 10(c) respectively show the numerical midspan lateral, vertical and torsional accelerations together with the full-scale response recorded on the bridge by the accelerometer "H5". To provide a detailed analysis of the response, the results are presented alongside the LF wind speed and AoA measured by the central anemometers. (i.e. "A5", "A6" and "A7", refer to [11]). The study focuses on a time window capturing the deck motion during the wind gust, specifically between 900s and 1400s.

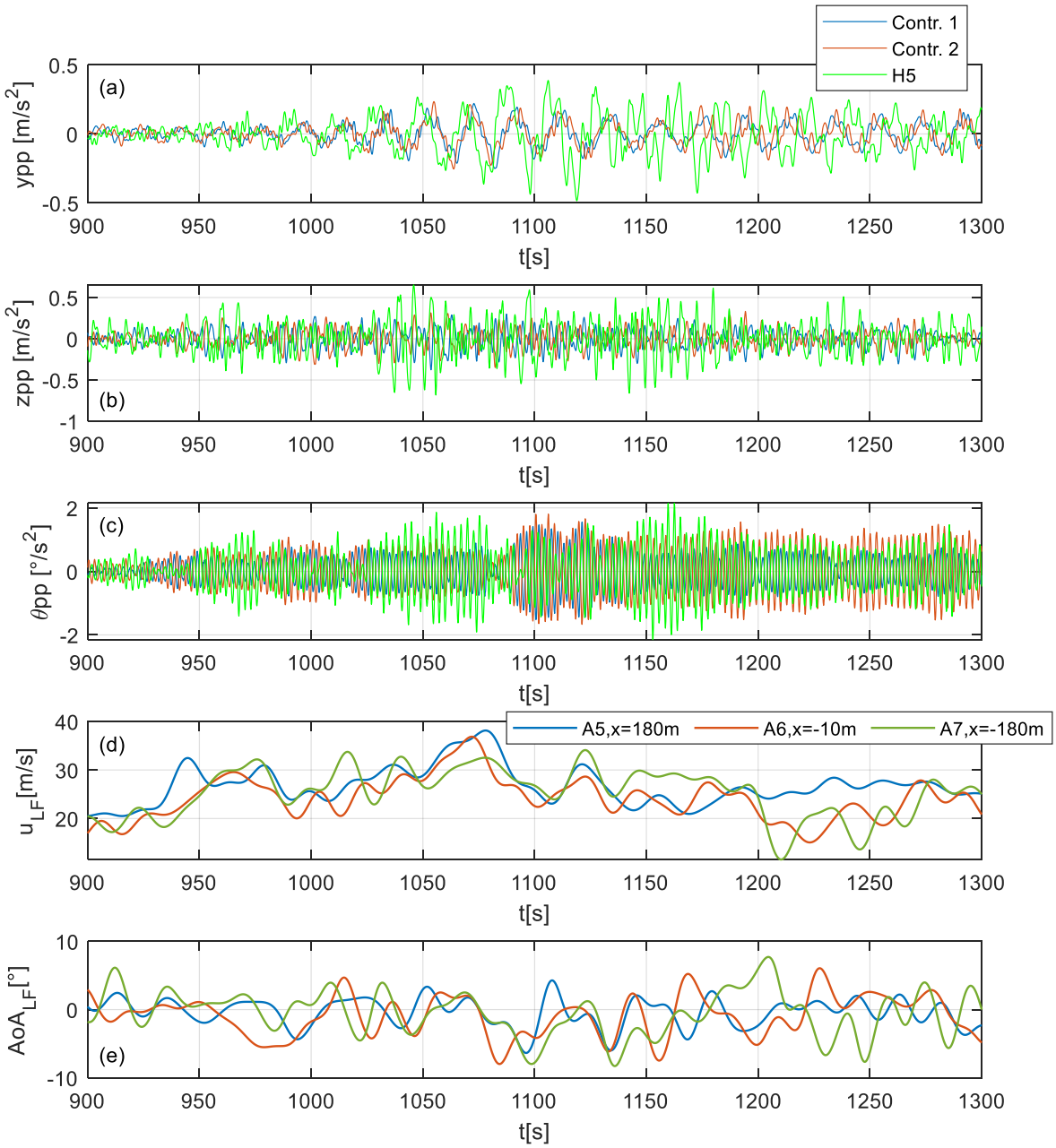

Figure 10. Midspan lateral, vertical and torsional accelerations, obtained by the participants, compared against the full-scale response measured on the bridge by the accelerometer "H5" (refer to [11]). The results are reported along with the LF wind speed and AoA recorded by the anemometers "A5", "A6" and "A7"

As first, it can be noted that the numerical results show a good agreement, highlighting the robustness of the nonlinear methods used for the calculations. Subsequently, consistently with the full-scale response, the lateral acceleration increases when there is a significant rise in the wind speed (i.e. between 1040 s and 1090 s). However, in the following instants, the experimental oscillations result higher than the numerical outputs. In the same time window, discrepancies are observed both in the vertical and torsional motion.

These differences may stem from the procedure used to generate the numerical non-synoptic wind scenario. Specifically, the HF wind portions were derived from the turbulence properties estimated using four closely spaced anemometers located in the half-span toward Bu (see Fenerci2018). However, non-synoptic events can exhibit highly localized characteristics that may vary significantly along the deck. With only two anemometers installed on the opposite half-span, approximately 200 m apart, accurately capturing the turbulence characteristics and their correlation is not feasible.

Another source of uncertainty lies in the aerodynamic admittance functions used to compute the buffeting forces. At low V^* values, the Davenport function $A(V^*)$, see Eq. (3), tends to significantly reduce the buffeting forces. However, this is not necessarily accurate. A dedicated experimental campaign would be required to properly define the admittance functions for this specific deck section.

In conclusion, given the uncertainties in the input data, particularly in the generation of the non-synoptic scenario and the aerodynamic admittance functions, this preliminary comparison can be considered reasonably good. However, further efforts are needed to achieve better agreement with the full-scale response.

6 References

[1] Andersen M.S., Isaksen B., Hansen S.O. Full-scale monitoring of the wind field, surface pressures and structural response of gjemnessund suspension bridge. *Structural Engineering International*. 2022; 32, 43–54.

[2] Barni N. et al. Time-variant self-excited force model based on 2d rational function approximation. *Journal of Wind Engineering and Industrial Aerodynamics.* 2021; 211, 104523.

[3] Barni N. et al. Buffeting response of a suspension bridge based on the 2d rational function approximation model for self-excited forces. *Engineering Structures.* 2022; 261, 114267.

[4] Calamelli F., Rossi R., Argentini T., Rocchi D., and Diana G. A nonlinear approach for the simulation of the buffeting response of long span bridges under non-synoptic storm winds. *Journal of Wind Engineering and Industrial Aerodynamics*. 2024; 247, 105681.

[5] Diana G. et al. An experimental validation of a band superposition model of the aerodynamic forces acting on multi-box deck sections. *Journal of Wind Engineering and Industrial Aerodynamics.* 2013; 113, 40–58.

[6] Diana G. et al. Wind tunnel: a fundamental tool for long-span bridge design. *Structure and Infrastructure Engineering*. 2015; 11, 533–555.

[7] Diana G. et al. Iabse task group 3.1 benchmark results. part 1: Numerical analysis of a two-degree-of-freedom bridge deck section based on analytical aerodynamics. *Structural Engineering International.* 2020a; 30, 401–410.

[8] Diana G. et al. Iabse task group 3.1 benchmark results. part 2: Numerical analysis of a three-degree-of-freedom bridge deck section based on experimental aerodynamics. *Structural Engineering International.* 2020b; 30, 411–420.

[9] Diana G. et al. Iabse task group 3.1 benchmark results. numerical full bridge stability and buffeting simulations. *Structural Engineering International*. 2022; 33(4), 623–634.

[10] Diana G. et al New challenges in the IABSE TG3.1 benchmark on super long span bridge aerodynamics. *Istanbul IABSE Symposium*. 2023, 285–293.

[11] Fenerci A., Øiseth O. Strong wind characteristics and dynamic response of a long-span suspension bridge during a storm. *Journal of Wind Engineering and Industrial Aerodynamics.* 2018; 172, 116–138.

[12] Zasso A. Flutter derivatives: Advantages of a new representation convention. *Journal of Wind Engineering and Industrial Aerodynamics.* 1996; 60, 35–47.

A more extensive and adequate bibliography can be found in [7,8,9].